CHEMISTRY OF MATERIALS

ARTICLE

pubs.acs.org/cm

Site-Specific Design of Cone-Shaped Si Nanowires by Exploiting Nanoscale Surface Diffusion for Optimal Photoabsorption

Jaeseok Yi, Dong Hyun Lee, and Won Il Park*

Division of Materials Science and Engineering, Hanyang University, Seoul 133-791, Korea

ABSTRACT: In this study, we introduce a new strategy to control silicon nanowire (SiNW) morphology (cone shape and cylindrical shape) by exploiting adatom diffusion at the nanostructured surface. In our approach, by using chemical treatment with a mixture of HF and H_2SO_4 acids, ordinary flat Si substrates were changed to nanoscale-faceted, corrugated surfaces, accompanied by a transition from a hydrophobic to hydrophilic surface. These nanostructured surfaces enhanced the surface diffusion, which eventually stimulated radial growth to change the NW morphology from a cylindrical shape to a cone shape with a sharp tip. By using site-specific chemical treatment, both cone-shaped and cylindrical-shaped SiNWs could be achieved selectively on the same chip under the same conditions. Furthermore, these shape-controlled SiNWs demonstrated an outstanding antireflection effect over a broad range of wavelengths, as determined by optical measurements and finite-difference time-domain modeling.

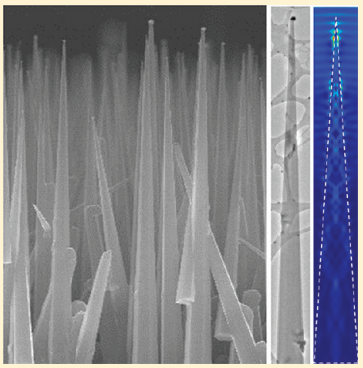

KEYWORDS: Si nanowires, nanocones, site-specific control, antireflection effect, nanoscale diffusion

INTRODUCTION

Since the vapor−liquid−solid (VLS) mechanism was proposed in 1964 as an explanation for silicon (Si) whisker formation, the growth of one-dimensional (1D) Si nanowires (SiNWs) has been extensively investigated.[1−4] Their unique electrical, optical, and mechanical properties, which are superior to their bulk counterparts, allow the use of 1D SiNWs as versatile building blocks for electronic and photonic devices, solar cells, and anodes for electrochemical energy storage applications.[5−11] Recently, particular attention has been paid to the enhancement of photoabsorption in SiNW solar cells by exploiting photon trapping and suppression of light reflection in three-dimensional arrays of 1D nanostructures.[12−17] Compared with conventional antireflection coatings that can only operate at specific wavelengths and incident angles, vertical arrays of SiNWs can offer opportunities to suppress surface reflection over a wide range of incident light wavelengths and angles. Specifically, cone-shaped SiNWs are of particular interest because their unique geometry is more suitable than cylindrical shaped SiNWs to achieve optimal photoabsorption. In these structures, a gradual change in the effective refractive index (n) from the refractive index of air ($n = 1$) to crystalline Si ($n = 4.1$) enables incident light to transmit the boundary between air and Si without considerable reflective losses.[18,19]

One approach to achieve 1D nanostructure arrays utilizes reactive ion etching of a planar wafer where a monolayer of micro- or nanospheres is generally used as an etching mask. In this approach, undercutting can be intentionally adopted to form tapered sidewalls with sharp tips through control of the etching conditions.[18,20−22] On the other hand, metal nanocluster-catalyzed chemical vapor deposition (CVD) has been developed to grow vertical arrays of various NWs.[1−3,17,23−25] Inspired by the fact that tapered nanowires (NWs) can be grown by radial overcoating at the sidewalls, the use of specific growth conditions can enable the direct growth of cone-shaped nanostructures. However, in these approaches, the radial growth generally yields amorphous and/or polycrystalline shell layers. In addition, control of the NW morphology is achieved only by managing global conditions such as temperature and vapor partial pressures, where site-specific control of these variables is often limited.[25−30] Furthermore, in addition to shape, other parameters such as the dimensions, density, and physical properties of NWs are very sensitive to the growth conditions. Therefore, in practice, precise control of each parameter without affecting the others is extremely challenging.

Here, we propose a new approach to control the shape of SiNWs by adjusting the surface of Si substrates. By using an appropriate chemical treatment, substrate surfaces can be controlled to be either atomically flat or nanoscale-faceted and rough. These surface structures may play an important role in nanoscale diffusion, which resulted in two distinctly different NW morphologies under the same growth conditions. Furthermore, through experimental and electromagnetic (EM) modeling results, the shape-controlled 1D nanostructures demonstrated an outstanding antireflection effect over a broad range of wavelengths.

EXPERIMENTAL SECTION

A metal nanocluster-catalyzed VLS method was used to grow single crystal SiNWs by using 20 nm diameter gold nanoparticles or ∼10 nm

Received: April 26, 2011
Revised: July 12, 2011
Published: August 04, 2011

ACS Publications © 2011 American Chemical Society

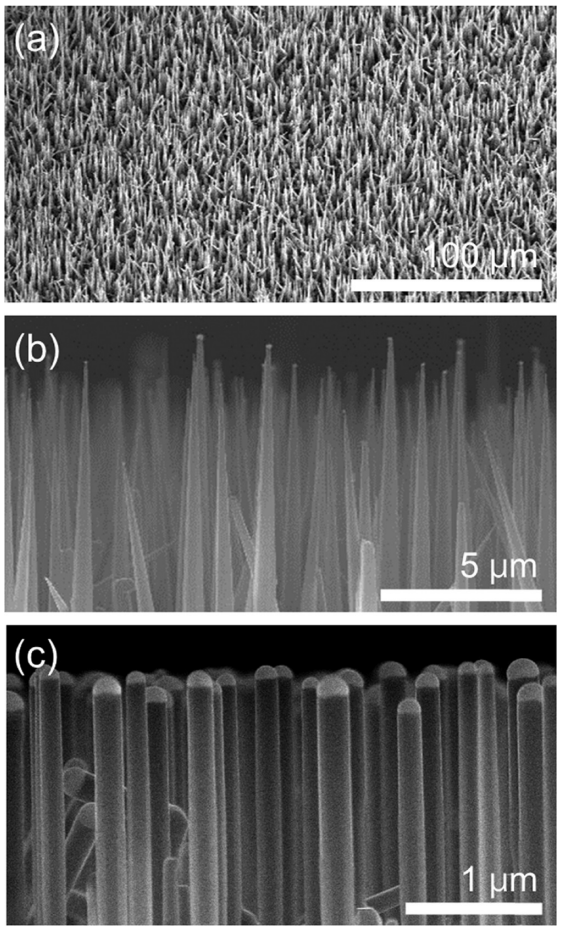

Figure 1. SEM images of vertically aligned SiNWs with different morphologies: (a, b) cone-shaped and (c) cylindrical-shaped SiNWs.

thick films deposited on ⟨111⟩ silicon substrates. Basically, the SiNW growth was performed by following the same procedures described in previous papers except for the substrate treatment step using chemical acids.[1−5,25−29] First, precut Si ⟨111⟩ substrates were sequentially cleaned ultrasonically in acetone, ethanol, and deionized (DI) water and then dried by N_2 blowing. Immediately after cleaning, the substrate surfaces were chemically etched by immersing into two types of solutions: 10% hydrofluoric (HF) acid, and a 4:1 (v:v) mixture of 49% HF and 97% sulfuric (H_2SO_4) acids. To obtain a net positively charged surface, the substrate was then immersed into a solution of poly-L-lysine (Sigma Aldrich), followed by deposition of gold nanoparticles (Sigma Aldrich, diluted to $\sim 2 \times 10^{11}$ particles/ml) and rinsing with DI water. The SiNW growth was carried out in a low pressure horizontal CVD system by using silane (SiH_4) as precursor. After placing the wafer in a quartz tube reactor, the reactor was evacuated to below 10^{-3} Torr, heated to 700−750 °C, and then maintained at that temperature for 10 min. After reaching the desired temperature, SiNW growth was performed for 0.5−2 h under SiH_4 and H_2 flows at a pressure of 5−10 Torr. As-grown SiNWs were examined by scanning electron microscopy (SEM) and transmission electron microscopy (TEM) to investigate their morphology, lengths, diameters, and crystallinity.

Reflectance of bare Si substrate and cone-shaped SiNWs was investigated by using an ultraviolet−visible−near infrared (UV−vis−NIR) spectrophotometer (Varian Cary 5000, Agilent) with reflectance accessory at 1 nm intervals in the wavelength range 300−800 nm. For the absolute values of reflectance, the measured spectra were normalized by Al mirror reference spectrum. To better understand the morphology dependent optical characteristics of the SiNWs, finite difference time-domain (FDTD) simulations were performed by using Lumerical FDTD solutions (version 7.0). In these simulations, the normalized reflection and transmission powers were calculated for a normally incident plane wave onto bare Si substrate and cone- and cylindrical- shaped SiNWs with center-to-center distance of 1.5 μm.

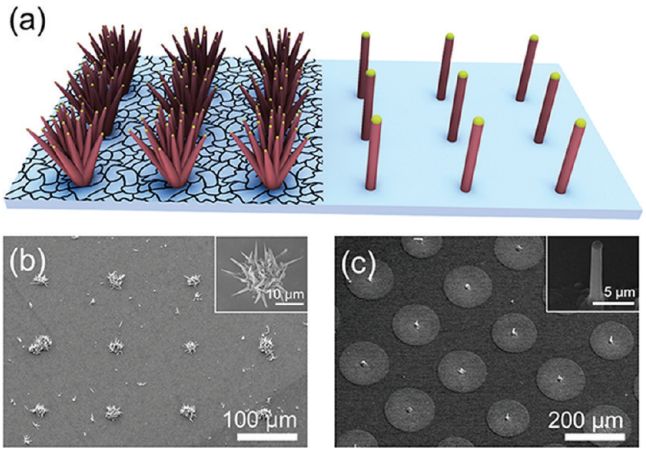

Figure 2. (a) Schematic illustrating the site- and shape-selective growth of SiNW arrays. SEM images of (b) a nanocone bundle and (c) cylindrical shaped SiNW arrays grown simultaneously.

RESULTS AND DISCUSSION

Figures 1a and b show SEM images of as-synthesized cone-shaped SiNWs (hereafter referred to as "Si nanocones") on Si substrates chemically etched with a mixture of HF and H_2SO_4 acids. The diameter of the nanocones gradually increased from top to bottom, which is distinctly different from the cylindrical shaped NWs, which have straight sidewalls and almost uniform diameters of ∼100−200 nm from the top to bottom (Figure 1c). While the diameter of the Si nanocone tips is comparable to that of the Au nanoclusters (100−200 nm) remaining at their ends, the bottom diameter depends on the growth time with an average base diameter of ∼1.5 μm for 30 min-grown, 15-μm-long Si nanocones.

To demonstrate site-specific control of the NW morphology, local chemical etching of the Si substrate surface was achieved by using a photolithographically defined passivation layer. Figure 2a schematically illustrates the simultaneous site- and shape-selective growth of NW arrays under the same growth conditions. While a cylindrical shaped SiNW array was achieved on the HF-treated region (Figure 2c), an array consisting of a nanocone bundle was formed on the region that was chemically etched by the HF and H_2SO_4 mixture (Figure 2b). This result clearly shows that the morphology of the 1D Si nanostructures can be selectively tuned by the use of a site-specific surface treatment strategy.

Further structural characterization of the Si nanocones was performed by TEM. The low magnification TEM image reveals that the Si nanocones have a high-aspect ratio and sharp tips with a cone angle below 5° (Figure 3a). A single crystal structure was also confirmed by the highly ordered lattice images in the high resolution TEM images (Figures 3b and c). The spacing of 0.314 nm between the lattice fringes corresponds to the *d*-spacing of the Si (111) planes, which indicates that Si nanocones grow along the [111] direction. In addition, this atomic configuration

dx.doi.org/10.1021/cm201188z |*Chem. Mater.* 2011, 23, 3902–3906

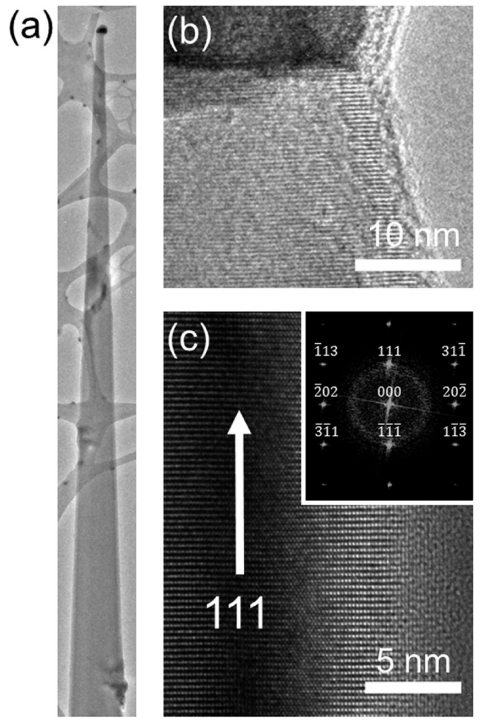

Figure 3. (a) Low-magnification TEM image of a Si nanocone. (b, c) High-resolution TEM images of different parts of the Si nanocone. In the inset, two-dimensional Fourier transforms of the lattice images depicting the $[\bar{2}11]$ zone axis the lattice fringes reveal that the NWs grew along the $\langle 111 \rangle$ orientation.

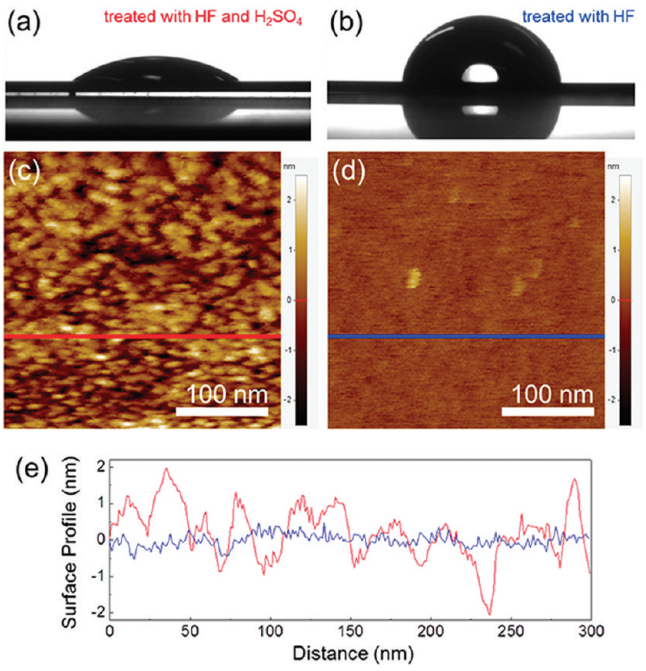

Figure 4. Photo images of static sessile water droplets on Si substrates treated with (a) a mixture of HF and H_2SO_4 acids, and (b) HF acid. AFM topography images of the Si substrates treated with (c) a mixture of HF and H_2SO_4 acids, and (d) HF acid. (e) AFM line profiles of the corresponding red and blue lines in (c) and (d), respectively.

continues from the bottom to top, from the center to the edge of the surface with no distinct defect or boundary.

In our case, the substrate surface treatment plays an important role in determining the NW morphology. To understand the underlying mechanism, the surface properties with the different chemical treatments were investigated. We first measured the wetting ability of the Si substrate surfaces by using the static sessile drop method. On the hydrophilic surface treated by HF and H_2SO_4, water droplets had a contact angle of ~30°. On the other hand, the substrate treated with HF had a much larger contact angle of ~83° (Figures 4a and b). The static contact angle (θ) results from the equilibrium interfacial energies, where mechanical equilibrium among three interfacial tensions yields Young's equation,[31,32]

$$(\gamma_{SV} - \gamma_{SL}) \cdot r = \gamma_{LV} \cdot \cos\theta \quad (1)$$

where γ_{SV}, γ_{SL}, and γ_{LV} are surface tensions at the solid−vapor, solid−liquid, and liquid−vapor interfaces, respectively. The surface roughness factor, r, is defined as the ratio of the area of the actual surface to that of a smooth surface with the same geometric dimensions. On the basis of this equation, the different wettabilities of the Si surfaces depending on the chemical treatment could be understood. The r value increased by a factor of 7 after surface treatment by the mixture of HF and H_2SO_4, corresponding to the increased surface roughness. The atomic force microscopy (AFM) images of the Si surfaces are also consistent with these results. The formation of a corrugated surface after treatment by the HF and H_2SO_4 mixture is obviously observed in the topographic image and line profile (Figure 4c and red line in Figure 4e), which is distinct from the HF-treated, flat surface (Figure 4d and blue line in Figure 4e).

In 1D nanostructure growth, there are two competing processes that can determine the shape of the nanostructures: axial growth governed by a metal nanocluster-catalyzed VLS mechanism and radial expansion driven by a vapor-solid (VS) process. The VLS process prevailing over the VS process results in the formation of NWs with a uniform diameter, while the VS-driven radial process accompanying axial VLS growth yields nanocone structures with a certain cone angle determined by the dominance of VS over VLS.[25,27,30,33] Taking the change of morphology of the NWs grown under the same conditions into account, it is deduced that the VS process is strongly related to the surface properties. In particular, the formation of nanocones on the corrugated surface suggests that the degree of surface roughness enhanced the diffusion of adatoms at the nanostructured surface, thereby promoted the VS process. Here, the diffusion of adatoms at the nanoscale surface would be affected by the size and shape of the surface structures,[34] where the temperature dependence of the diffusion coefficient, D_{adatom}, is governed by[35]

$$D_{adatom} = D_0 \cdot e^{\left(-\frac{Q_{adatom}}{RT}\right)} \quad (2)$$

where D_0 is a temperature-independent pre-exponential factor, Q_{adatom} is the activation energy for surface diffusion, R is the ideal gas constant, and T is the absolute temperature. Q_{adatom}, the activation energy for surface diffusion, is determined by

$$Q_{adatom} = C_{adatom} \cdot T_m \quad (3)$$

where C_{adatom} is the coefficient for surface diffusion and T_m is the melting temperature at the nanoscale. On the logarithmic scale, D_{adatom} is inversely proportional to T_m. Taking the size and shape

dx.doi.org/10.1021/cm201188z |Chem. Mater. 2011, 23, 3902–3906

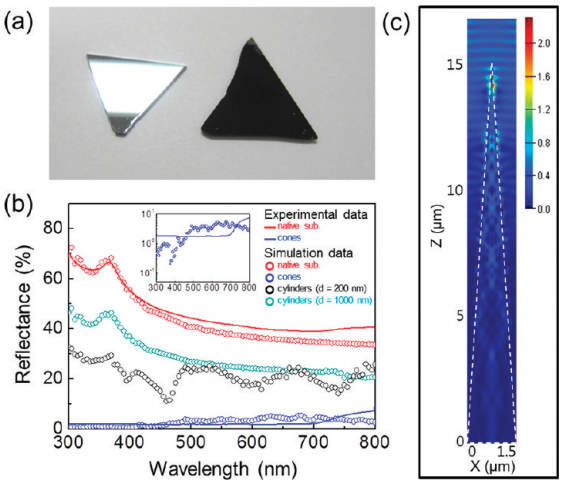

Figure 5. (a) Photographs of a bare Si substrate (left) and nanocone arrays (right) under white light illumination. (b) Experimental (lines) and simulated (circles) reflectance spectra of a Si substrate (red), Si nanocones (blue), and Si nanocylinders (the black and green circles correspond to diameters of 200 and 1000 nm, respectively). Inset, reflectance spectra of Si nanocones plotted in log scale. (c) Simulated electric field distribution for 800 nm wav elength propagating light in a Si nanocone.

effects on the melting point at the nanoscale into account leads to the following thermodynamic expression,[34,36−38]

$$T_m = T_0\left[1 - \left(\frac{\gamma_{LV} - \gamma_{SV}}{\Delta H_0}\right)\frac{A}{V}\right] \quad (4)$$

where T_0 and ΔH_0 are the melting temperature and the melting enthalpy of the bulk material, respectively, and A/V is the surface to volume ratio. In this equation, it is important to note that as the size decreases or the surface gets rougher, the surface to volume ratio, A/V, increases and thus, causes a decrease of T_m, as compared to its bulk counterpart. By combining eqs 2−4, it can be deduced that the enlarged surface area of the corrugated surface would decrease T_m and, as a result, the adatom diffusion becomes faster, which eventually stimulates the VS process to promote nanocone growth.

Figure 5a shows a photograph of a bare Si ⟨111⟩ substrate and nanocone arrays under white light illumination, which clearly reveals their different light reflection characteristics. Because of the high refractive index of crystalline Si, the flat Si substrate is mirror-like and highly reflective. On the other hand, the Si nanocone array is extremely dark colored, which demonstrates that these nanostructures effectively suppress the reflection of light in the visible spectral range. The measurement results of the optical reflection spectra correspond with this phenomenon (Figure 5b). The average reflection value of the nanocone array in the range of 300−800 nm is ∼2.4%, which is significantly lower than that of the native Si substrate (∼47%) and comparable to those of cone- or needle-shaped 1D nanostructures (hydrogenated amorphous Si nanocone array ∼7%, Ge nanoneedles below 1%).[17,18] To better understand the antireflection effect of the nanocone array, FDTD analysis was carried out on the flat Si surface and a periodic array of nanocones with a height of 15 μm and a cone angle of 5°. The simulation results (red and blue circles in Figure 5b) agree well with the experimental reflectance spectra (red and blue lines). The average simulated reflectance values for the substrate and nanocone array are 44% and 2.7%, respectively. In addition, to reveal the propagation behavior of incident light in the nanocone array, the distribution of the electric field intensity for 800 nm wavelength EM waves is shown in Figure 5c. Because of the optical absorption of nanocone, the electric field intensity of the EM waves gradually decreased along the surface of the nanocones and most of the electric intensity disappeared at the bottom region of the nanocones. Our calculations revealed that only 1.2% of the initial light can escape from the Si nanocones. Considering that the intensity of incident light must equal the sum of the reflected, transmitted, and absorbed light, it was deduced that the Si nanocones absorbed over 96% of light in the visible spectral range.

We also investigated the nanostructure morphology dependence on the optical characteristics. The cylindrical shaped NWs with diameters of 200 and 1000 nm were considered as representative components of the arrays while the interwire distance and length were kept the same as those of the nanocone array. The calculated results show that cylindrical NW arrays exhibited average reflection values of 22% for 200 nm diameter NWs and 29% for 1000 nm diameter NWs (green and black circles in Figure 5b), which is 1 order of magnitude higher than that of the nanocones. Moreover, the optical absorption of the cylindrical NW arrays was calculated to be in the range of 49−64%. Therefore, we can conclude that the nanocone array exhibited a drastic improvement in the optical absorption characteristics compared to cylindrical NWs.

CONCLUSIONS

In conclusion, a new approach for controlled synthesis of vertical SiNWs with a tunable morphology was demonstrated by exploiting the surface diffusion of adatoms depending on the surface nanostructure. Specifically, the radial expansion driven by the VS process with enhanced surface diffusion on the corrugated surface accompanying axial VLS growth yielded nanocone structures. The dependence of the NW shape on the surface properties was further exploited to achieve site-specific growth of NW arrays with two distinctly different NW shapes by the use of a local surface treatment strategy. We also demonstrated that the Si nanocone array exhibited significantly improved antireflection characteristics compared to the cylindrical shaped NW array, leading to an optical absorption of 96% for incident light over a broad range of wavelengths. Although this study was restricted to the growth of SiNWs, the synthetic mechanism which exploits nanoscale surface diffusion may be readily expanded to control the shape and size of many other semiconductor nanostructures.

AUTHOR INFORMATION

Corresponding Author

*E-mail: wipark@hanyang.ac.kr.

ACKNOWLEDGMENT

This work was supported by a KIST research program (grant no. 2E22121) and by Future-based Technology Development Program (Nano Fields) through the National Research Foundation of Korea (NRF) funded by the Ministry of Education, Science and Technology (2010-0029300).

REFERENCES

(1) Wagner, R. S.; Ellis, W. C. *Appl. Phys. Lett.* **1964**, *4*, 89–90.
(2) Hochbaum, A. I.; Fan, R.; He, R.; Yang, P. *Nano Lett.* **2005**, *5*, 457–460.
(3) Hannon, J. B.; Kodambaka, S.; Ross, F. M.; Tromp, R. M. *Nature* **2006**, *440*, 69–71.
(4) Park, W. I.; Zheng, G.; Jiang, X.; Tian, B.; Lieber, C. M. *Nano Lett.* **2008**, *8*, 3004–3009.
(5) Goldberger, J.; Hochbaum, A. I.; Fan, R.; Yang, P. *Nano Lett.* **2006**, *6*, 973–977.
(6) Wu, X.; Kulkarni, J. S.; Collins, G.; Petkov, N.; Almeécija, D.; Boland, J. J.; Erts, D.; Holmes, J. D. *Chem. Mater.* **2008**, *20*, 5954–5967.
(7) Shan, Y.; Fonash, S. J. *ACS Nano* **2008**, *2*, 429–434.
(8) Cui, Y.; Lieber, C. M. *Science* **2001**, *291*, 851–853.
(9) Tian, B.; Zheng, X.; Kempa, T. J.; Fang, Y.; Yu, N.; Yu, G.; Huang, J.; Lieber, C. M. *Nature* **2007**, *449*, 885–889.
(10) Shiu, S.-C.; Chao, J.-J.; Hung, S.-C.; Yeh, C.-L.; Lin, C.-F. *Chem. Mater.* **2010**, *22*, 3108–3113.
(11) Chan, C. K.; Peng, H.; Liu, G.; McIlwrath, K.; Zhang, X. F.; Huggins, R. A.; Cui, Y. *Nat. Nanotechnol.* **2008**, *3*, 31–35.
(12) Peng, K.; Xu, Y.; Wu, Y.; Yan, Y.; Lee, S.-T.; Zhu, J. *Small* **2005**, *1*, 1062–1067.
(13) Lee, Y.-J.; Ruby, D. S.; Peters, D. W.; McKenzie, B. B.; Hsu, J. W. P. *Nano Lett.* **2008**, *8*, 1501–1505.
(14) Cansizoglu, M. F.; Engelken, R.; Seo, H.-W.; Karabacak, T. *ACS Nano* **2010**, *4*, 733–740.
(15) Wu, C.-T.; Lin, C.-H.; Cheng, C.; Wu, C.-S.; Ting, H.-C.; Chang, F.-C.; Ko, F.-H. *Chem. Mater.* **2010**, *22*, 6583–6589.
(16) Fan, Z.; Kapadia, R.; Leu, P. W.; Zhang, X.; Chueh, Y.-L.; Takei, K.; Yu, K.; Jamshidi, A.; Rathore, A. A.; Ruebusch, D. J.; et al. *Nano Lett.* **2010**, *10*, 3823–3827.
(17) Chueh, Y.-L.; Fan, Z.; Takei, K.; Ko, H.; Kapadia, R.; Rathore, A. A.; Miller, N.; Yu, K.; Wu, M.; Haller, E. E.; Javey, A. *Nano Lett.* **2009**, *10*, 520–523.
(18) Zhu, J.; Yu, Z.; Burkhard, G. F.; Hsu, C.-M.; Connor, S. T.; Xu, Y.; Wang, Q.; McGehee, M.; Fan, S.; Cui, Y. *Nano Lett.* **2008**, *9*, 279–282.
(19) Jung, J.-Y.; Guo, Z.; Jee, S.-W.; Um, H.-D.; Park, K.-T.; Lee, J.-H. *Opt. Express* **2010**, *18*, A286–A292.
(20) Wang, Y.; Lu, N.; Xu, H.; Shi, G.; Xu, M.; Lin, X.; Li, H.; Wang, W.; Qi, D.; Lu, Y.; et al. *Nano Res.* **2010**, *3*, 520–527.
(21) Hsu, C.-M.; Connor, S. T.; Tang, M. X.; Cui, Y. *Appl. Phys. Lett.* **2008**, *93*, 133109–133103.
(22) Isa, L.; Kumar, K.; Mùller, M.; Grolig, J.; Textor, M.; Reimhult, E. *ACS Nano* **2010**, *4*, 5665–5670.
(23) Lombardi, I.; Hochbaum, A. I.; Yang, P.; Carraro, C.; Maboudian, R. *Chem. Mater.* **2006**, *18*, 988–991.
(24) Wan, Q.; Wei, M.; Zhi, D.; MacManus-Driscoll, J. L.; Blamire, M. G. *Adv. Mater.* **2006**, *18*, 234–238.
(25) Krylyuk, S.; Davydov, A. V.; Levin, I. *ACS Nano* **2010**, *5*, 656–664.
(26) Bootsma, G. A.; Gassen, H. J. *J. Cryst. Growth* **1971**, *10*, 223–234.
(27) Sharma, S.; Kamins, T. I.; Williams, R. S. *J. Cryst. Growth* **2004**, *267*, 613–618.
(28) Cao, L.; Garipcan, B.; Atchison, J. S.; Ni, C.; Nabet, B.; Spanier, J. E. *Nano Lett.* **2006**, *6*, 1852–1857.
(29) Bae, J.; Kulkarni, N. N.; Zhou, J. P.; Ekerdt, J. G.; Shih, C.-K. *J. Cryst. Growth* **2008**, *310*, 4407–4411.
(30) Woo, R. L.; Gao, L.; Goel, N.; Hudait, M. K.; Wang, K. L.; Kodambaka, S.; Hicks, R. F. *Nano Lett.* **2009**, *9*, 2207–2211.
(31) Wenzel, R. N. *J. Phys. Colloid Chem.* **1949**, *53*, 1466–1467.
(32) Young, T. *Phil. Trans.* **1805**, *95*, 65–87.
(33) Cho, H. S.; Kamins, T. I. *J. Cryst. Growth* **2010**, *312*, 2494–2497.
(34) Guisbiers, G.; Buchaillot, L. *Nanotechnology* **2008**, *19*, 435701.
(35) Ohring, M. *Materials Science of Thin Films: Deposition and Structure*; Academic Press: San Diego, CA, 2002.
(36) Wautelet, M. *Nanotechnology* **1992**, *3*, 42.
(37) Wautelet, M. *Phys. Lett. A* **1998**, *246*, 341–342.
(38) Guisbiers, G.; Kazan, M.; Van Overschelde, O.; Wautelet, M.; Pereira, S. *J. Phys. Chem. C* **2008**, *112*, 4097–4103.